Article

Hanging Photothermal Fabric Based on Polyaniline/Carbon Nanotubes for Efficient Solar Water Evaporation

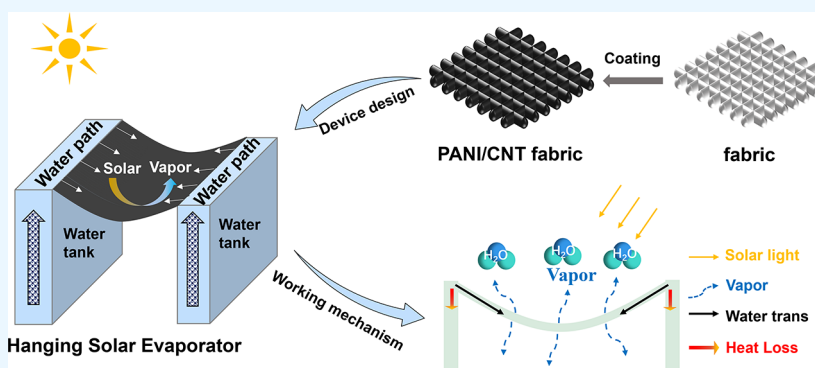Daiyi Wang, Xiaofeng Lin, Yujian Wu, Luxin Li, Wei Feng, Yanyan Huang, and Yuxin Yang*

Read Online

ACCESS | Metrics & More | Article Recommendations | Supporting Information

ABSTRACT: Solar-driven water evaporation is essential to provide sustainable and ecofriendly sources of fresh water. However, there are still great challenges in preparing materials with broadband light absorption for high photothermal efficiency as well as in designing devices with large evaporation areas and small heat dissipation areas to boost the water evaporation rate. We designed a hanging-mode solar evaporator based on the polyaniline/carbon nanotube (PANI/CNT) fabric, in which the photothermal fabric acts as the solar evaporator and the micropores on the cotton fabric act as the water transfer channels. The hanging mode provides efficient evaporation at both interfaces by greatly reducing the heat dissipation area. The hanging mode PANI/CNT fabric solar evaporator can achieve an evaporation rate of 2.81 kg·m^{-2}·h^{-1} and a photothermal efficiency of 91.74% under a solar illumination of 1 kW·m^{-2}. This high-performance evaporator is designed by regulating the photothermal material and evaporation device, which provides a novel strategy for sustainable desalination.

■ INTRODUCTION

Fresh water is an important natural resource for human survival. Solar-driven water evaporation to produce high-quality fresh water by converting light energy into heat through the photothermal effect has become a very promising technology.[1−4] The key to this process is the manufacture of highly efficient photothermal materials, followed by effective interfacial thermal management and conversion during solar evaporation.[5−9]

In previous studies, a single interfacial evaporation layer was prepared by using photothermal nanomaterials for water evaporation under solar irradiation. Photothermal nanomaterials are classified into organic polymer materials (PANI,[10−12] PPy,[13−15] etc.), metal nanomaterials (Cu,[16,17] Au,[18,19] etc.), carbon-based materials (CNT,[20−22] CB,[23,24] etc.), semiconductive materials (MoS$_2$,[25,26] CuS,[27,28] etc.), and MXene.[29] Compared to metal nanomaterials, PANI and CNT have excellent light absorption because of their black appearance and can transform the absorbed light energy into thermal through phonon scattering or lattice vibration.[30−34] Li et al. prepared PANI membranes by an immersion precipitation phase inversion method and modified the membranes with acid doping, which resulted in an improved hydrophilicity and a water evaporation rate and photothermal efficiency of up to 1.38 kg·m^{-2}·h^{-1} and 80.7%, respectively.[12] Zhu et al. designed a CNT-embedded polyacrylonitrile nonwoven fabric that exhibited a 90.8% light absorption in the spectral range (350−2500 nm) and showed an evaporation rate of 1.44 kg·m^{-2}·h^{-1} under 1 kW·m^{-2} sunlight irradiation.[20] Carbon-based materials are also widely used in photothermal applications to improve evaporation performance, as they are more stable than polymers and can easily form a variety of structures in macro-, micro-, and nanomorphologies.[35−38] Furthermore, there are relatively fewer studies of PANI/CNT composites for interfacial photothermal water evaporation, and
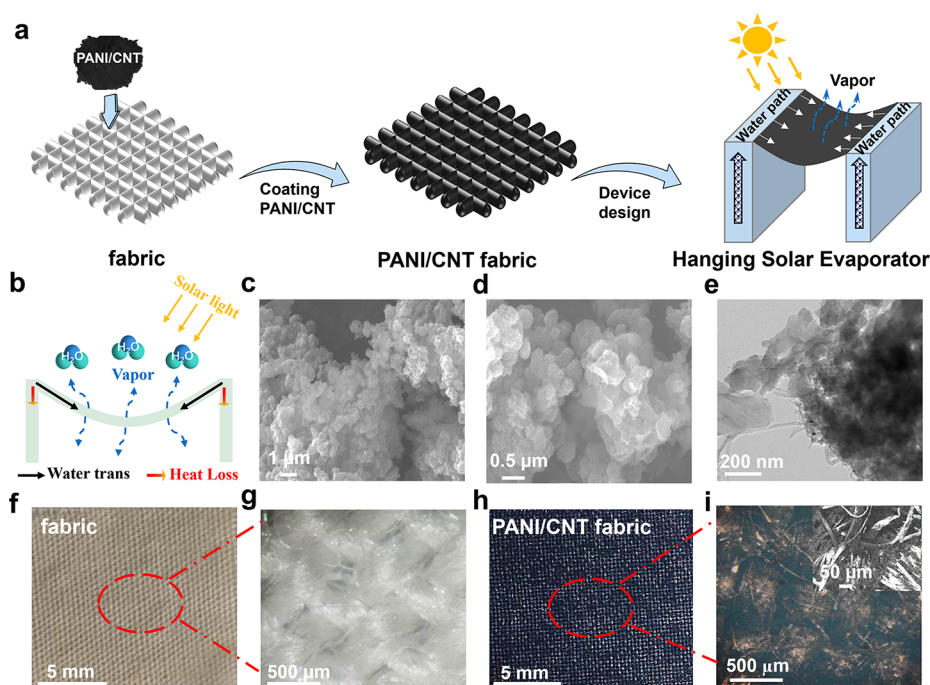
Figure 1. (a) Schematic diagram of PANI/CNT fabric preparation and interfacial evaporation. (b) Illustration of the working mechanism of the hanging-mode solar evaporator. (c, d) SEM images of PANI/CNT. (e) TEM images of PANI/CNT. Physical image (f) and microscope image (g) of the white cotton fabric. Physical image (h) and microscope image (i) of the PANI/CNT fabric.

the related interfacial design and performance optimization still have great research prospects.

This form of a single interfacial solar evaporation layer greatly increases the evaporation rate compared to bulk heating, but the entire bottom of the photothermal membrane is in direct contact with the bulk water and has a large heat dissipation area.[39−41] To reduce heat dissipation, photothermal layers are designed as multilayered or porous structures.[42−49] However, photothermal layers still have unavoidable heat loss to bulk water. To further improve the evaporation rate, the evaporation interface can be separated from the original bulk water surface to obtain better solar radiation concentration, such as jellyfish mode, hollow cone mode, arch mode, hanging mode, etc.[50−57] In one of them, Liu et al. used a polyaniline-coated cotton fabric that was hung in an arc mode with the central portion lingering in the air, which exhibited efficient double-surface evaporation at a rate of 1.94 kg·m^{-2}·h^{-1} under a solar illumination of 1.0 kW·m^{-2}.[56] Therefore, utilizing the most potential photothermal material of PANI/CNT to design photothermal devices with large evaporation areas and small heat dissipation areas is a great way to improve the evaporation rate.

Herein, we present a hanging-mode photothermal fabric by using PANI/CNT composites through a simple and scalable dip-coating method that exhibits efficient light absorption, photothermal efficiency, and water transport capacity. The PANI/CNT fabric acts as a solar absorber and evaporator, and both ends of the fabric adsorb water by capillary action and then gradually transfer it to the photothermal layer. The use of an indirect evaporation system with such an interface as a hanging mode is helpful in reducing heat loss into bulk water and in realizing efficient evaporation with a double interface. The hanging photothermal evaporator based on the PANI/CNT fabric can achieve an evaporation rate of 2.81 kg·m^{-2}·h^{-1} and a photothermal efficiency of 91.74% under a solar

illumination of 1 kW·m^{-2}. This high-performance evaporator is designed by regulating the photothermal material, and the evaporation device brings a way to take full advantage of solar energy and provides new ideas for sustainable desalination.

■ RESULTS AND DISCUSSION

This work aimed to develop a hanging-mode PANI/CNT photothermal fabric as an efficient solar-driven interfacial evaporation device to obtain fresh water. As schematically illustrated in Figure 1a, we loaded PANI/CNT powder onto a fabric via the dip-coating method and designed the evaporation device as a hanging mode. The two ends of the photothermal fabric act as the water paths and are immersed in two water tanks. The water is transferred to the photothermal interface for water evaporation by the capillary action of the fabric. In this mode, the heat loss area is greatly reduced because only the two ends are connected to the water bulk (Figure 1b). At the same time, the hanging design can increase the area of photothermal conversion and have a double-sided photothermal evaporation area. The PANI/CNT powder was prepared by chemical oxidation, which is mostly nanosheets with particles accumulating in a reef shape (Figure 1c,d). And the successful synthesis of PANI/CNT was further confirmed by XRD patterns (Figure S1). Figure 1e shows that the CNTs are well encapsulated by PANI. The white cotton fabric (Figure 1f) was chosen as the substrate because of its low cost, high textural porosity and hydrophilicity, and the viability of mass production. The fabrics are woven from fiber bunches (diameter ≈ 190 μm) with an extensive surface area. In addition, the surface of the fiber is very smooth (Figure 1g). The application of the prepared slurry onto the fabric not only serves to support the photothermal material but also gives it a certain roughness as well as a good hydrophilic and porous structure (Figure S2). After coating, the dried PANI/CNT fabric shows a dark color (Figure 1h,i), which greatly improves
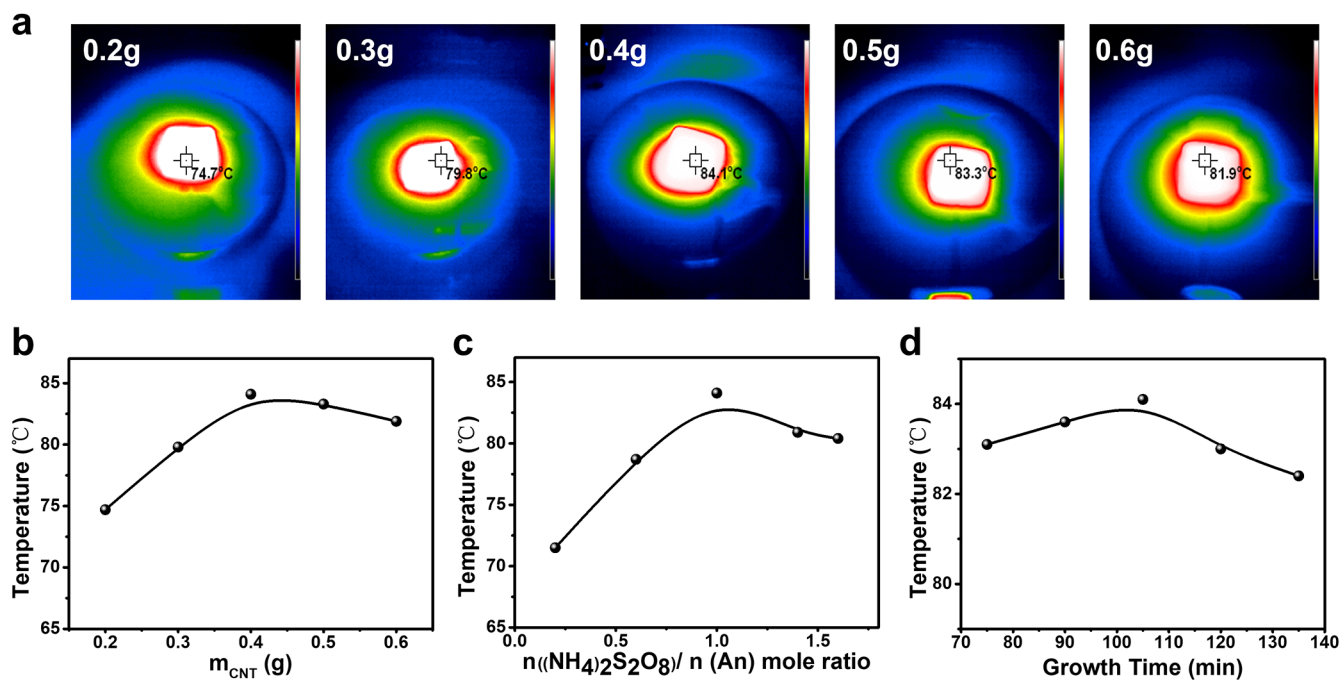
Figure 2. (a) Infrared images of the PANI/CNT fabric at different weights of the CNT. Temperature of the PANI/CNT fabric at (b) different weights of the CNT, (c) different $n((NH_4)_2S_2O_8)/n(An)$, and (d) different growth times.
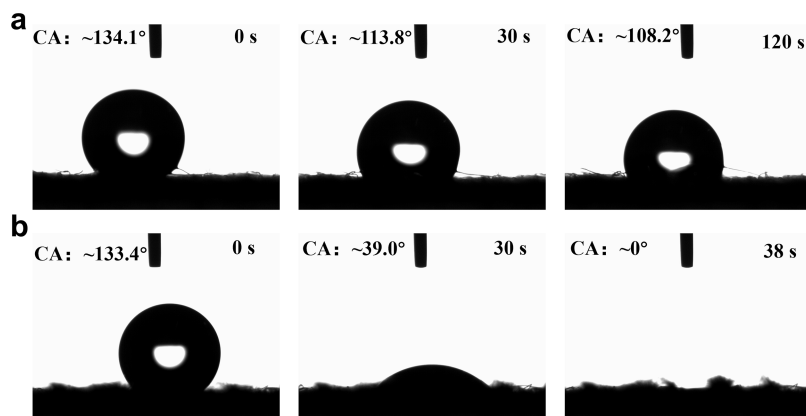

Figure 3. (a) Photographs of the water droplet on a white cotton fabric at 0, 30, and 120 s. (b) Photographs of the water droplet on a PANI/CNT fabric at 0, 30, and 38 s.

the light absorption of the fabric. Therefore, the above results indicate that PANI/CNT has a good decorative effect on cotton fabrics.

The photothermal properties of the PANI/CNT fabric can be adjusted by different reaction conditions, such as the weight of the CNT, growth time, and $n((NH_4)_2S_2O_8)/n(An)$ ratio. The surface temperatures of the PANI/CNT fabric with different weights of the CNT were recorded by infrared imaging (Figure 2a). The surface temperature of the PANI/CNT fabric initially rose and then diminished as further CNT was incorporated, reaching the maximum photothermal temperature of 84.1 °C at 0.4 g, as demonstrated in Figure 2b. When the weight of the CNT exceeded 0.4 g, the photothermal temperature started to decrease.

By increasing the $n((NH_4)_2S_2O_8)/n(An)$ mole ratios, the photothermal temperature increases initially and then subsequently decreases, reaching the maximum photothermal temperature at a mole ratio of 1.0, as illustrated in Figure 2c

and Figure S3. When the molar ratio used exceeds 1.0, the photothermal temperature decreases. This is because the excess APS further oxidizes the polyaniline with an emerald green imine type structure to non-emerald green imine type[58] and also leads to low-molecular-weight compounds,[59] thus affecting its photothermal performance.

As shown in Figure 2d and Figure S4, the surface temperature reached the maximum photothermal temperature of 84.1 °C at 105 min. The photothermal temperature decreases when the reaction time exceeds 105 min. The main reason is that the growth time affects the polymerization reaction process of PANI/CNT. When the time exceeds 105 min, the photothermal temperature decreases. Long-time reactions can cause some disruption of the molecular chain conjugation structures that have already formed, which will reduce its photothermal performance.[60,61] Therefore, through condition regulation, we can well improve the photothermal performance of the PANI/CNT fabric and further optimize the

interfacial photothermal layer to obtain the excellent performance of photothermal functional fabrics.

Good hydrophilicity is a prerequisite for achieving a good water supply to the light-absorbing layer during water evaporation. To verify the hydrophilicity of photothermal fabrics, contact angle experiments were conducted. It was found that the water contact angle of the white cotton fabric exceeded 90°, which was in a nonwetting state and had poor hydrophilicity (Figure 3a). On the contrary, the water contact angle of the PANI/CNT fabric gradually decreased with the extension of time. The water contact angle is 39° at 30 s, which proves that the water drops on the fabric surface have been partially absorbed and are in a partially wetted state. The water contact angle was equal to 0° at 38 s, proving that the PANI/CNT fabric was greatly hydrophilic and in a completely wetted state (Figure 3b). This is because PANI and CNT are modified on a white cotton fabric, which improves the surface roughness and increases the specific surface area, thus increasing the absorption capacity of water. Thus, it is better to simultaneously achieve good photothermal performance and hydrophilicity via loading PANI/CNT on a white cotton fabric, which is more favorable for solar evaporation.

On this basis, the photothermal properties of PANI, CNT, and PANI/CNT materials were further investigated. The IR thermal images of the PANI fabric, CNT fabric, and PANI/CNT fabric are shown in Figure S5. As shown in Figure 4a, the
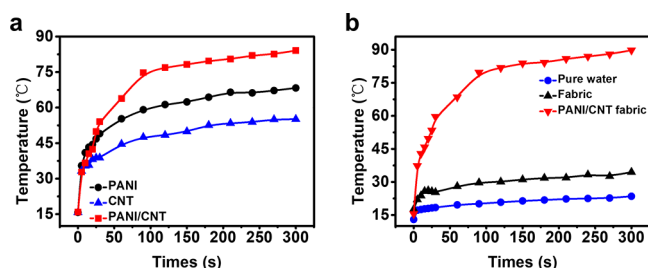

Figure 4. (a) Temperature of the PANI fabric, CNT fabric, and PANI/CNT fabric within 300 s under the infrared light source. (b) Temperature of the pure water, fabric, and PANI/CNT fabric within 300 s under the infrared light source.

surface temperature of the fabric increased to 68.3 °C after loading PANI, 55.1 °C after loading CNT, and 84.1 °C after loading PANI/CNT. It can be observed that the surface temperatures of PANI fabric, CNT fabric, and PANI/CNT fabric surfaces all gradually increased with time. However, the surface temperature of the PANI/CNT fabric rises faster and higher, further confirming that the PANI/CNT composite has higher light absorption and photothermal conversion ability than PANI and CNT.

Solar-driven water evaporation technology uses photothermal materials to transform the received light energy into thermal energy, which is further used to heat the liquid at the fabric–air interface for efficient water evaporation. To characterize the photothermal conversion performance of the PANI/CNT fabric, the surface temperature changes of pure water, fabric, and PANI/CNT fabric under a solar illumination of 1 kW·m^{-2} were measured in real time by infrared thermography (Figure S6). Figure 4b shows that the temperature of the PANI/CNT fabric surface increased rapidly with time, and the highest photothermal temperature reached 89.8 °C at 300 s. The temperature of pure water hardly

changed with time and the temperature of the blank cotton fabric surface increased slowly and was 34.5 °C at 300 s. It indicates that the cotton fabric modified by PANI/CNT has more excellent light absorption and presents better photothermal efficiency.

To investigate the effect of different evaporation systems on water evaporation performance, a solar-driven water evaporation experiment with a hanging photothermal fabric device was constructed. The results indicate that the weight loss of the pure water evaporation system under dark conditions is extremely small, reflecting the natural evaporation of water. Meanwhile, the weight loss of the PANI/CNT fabric evaporation system is much larger than that of the pure water and fabric system under the same conditions (Figure 5a). This is due to the capillary action and hydrophilicity of the composite photothermal fabric, which transported water to the surface of the fabric continuously and accelerated water evaporation. And their corresponding water evaporation rates were calculated from the weight loss. The evaporation rates of the white cotton fabric and PANI/CNT fabric were 1.35 and 2.81 kg·m^{-2}·h^{-1}, respectively, which were significantly higher compared to pure water (evaporation rate 0.09 kg·m^{-2}·h^{-1}) (Figure 5b). And the photothermal efficiencies (η) were calculated according to eq 1:[62,63]

$$\eta = mh_{LV}/q_i \qquad (1)$$

where m is the light-induced evaporation rate (kg·m^{-2}·h^{-1}); q_i represents the incident solar intensity (kW·m^{-2}); and h_{LV} denotes the total enthalpy of the liquid–vapor phase change of water (kJ·kg^{-1}), including sensible and latent heat enthalpy, which can be calculated as eq 2:

$$h_{LV} = \lambda_{LV} + C_p \Delta T \qquad (2)$$

where λ_{LV} is the latent heat of vaporization of water at standard atmospheric pressure (2.257 MJ·kg^{-1}); C_p is the specific heat capacity of water (4.2 kJ·kg^{-1}·K^{-1}); and ΔT is the temperature rise of water (K). For bare pure water, η is very low and calculated to be 38.96% under one sun. When the evaporator is used, the photothermal efficiency remarkably increases to 91.74% (Figure S7). In addition, the condensate produced is well below the threshold salinity for freshwater taste, as defined by the World Health Organization (Na$^+$ < 200 mg·L^{-1}) (Figure S8). It can be seen that the hanging-mode PANI/CNT fabric has high solar energy utilization, higher photothermal conversion performance, and better evaporation performance.

Usually, a higher light intensity always confers faster evaporation rates. The water evaporation performance under different light intensities was also investigated. When the light intensity further increased to 3 and 5 kW·m^{-2}, the weight loss of the PANI/CNT fabric was greatly increased (Figure 5c). The evaporation rates go up to 3.67 and 4.50 kg·m^{-2}·h^{-1}, respectively (Figure 5d). It can be seen that the evaporation rate is positively correlated with light intensity, which also indicates that the hanging-mode PANI/CNT fabric can ensure high water evaporation efficiency under high light intensity.

The reusability and durability of the solar steam devices are critical for their practical evaporation applications. First, we conducted 10 consecutive cycle tests. As shown in Figure 5e, there is no significant decrease in the evaporation rate, and the water evaporation rate is approximately stable at about 2.61 kg·m^{-2}·h^{-1}. To reveal the practical applications of our solar steam device in a real environment, we set up the device to conduct
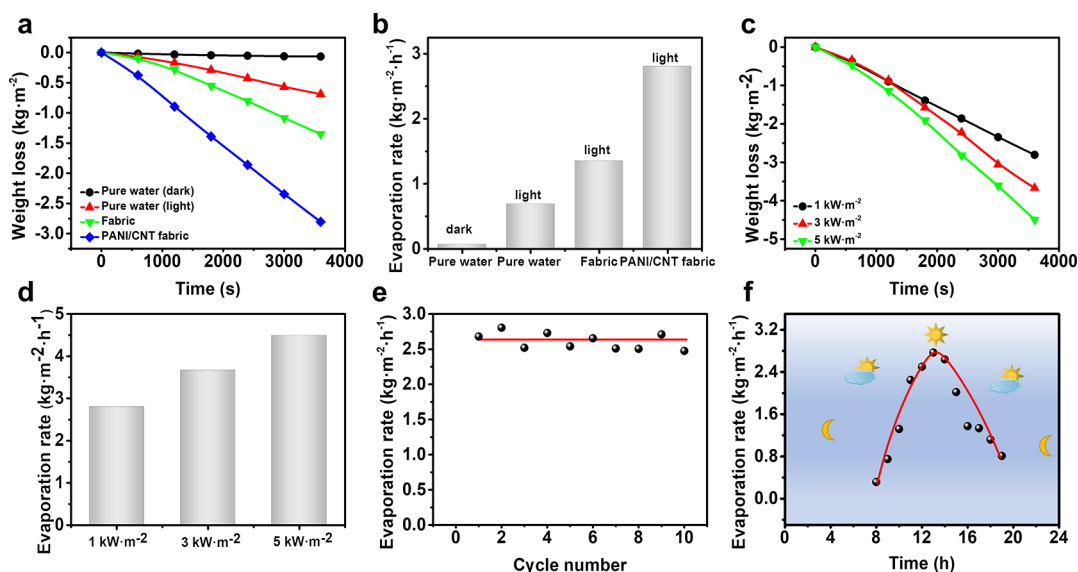
Figure 5. Water evaporation performance of photothermal fabrics. (a) Weight loss and (b) evaporation rate of different evaporation systems under a solar illumination of 1 kW·m^{-2}. (c) Weight loss and (d) evaporation rate of the PANI/CNT fabric under different light intensities. (e) Cycling test of solar steam devices. (f) Outdoor test of solar steam devices.

outdoor experiments with the PANI/CNT fabric and natural sunlight (7:00−19:00, 18 August 2023). We monitored the change in water evaporation over time (Figure 5f). The results showed that the water evaporation rate gradually increased from 0.315 kg·m^{-2}·h^{-1} at 8:00 to 2.77 kg·m^{-2}·h^{-1} at 13:00 and then decreased to 0.81 kg·m^{-2}·h^{-1} at 19:00. This was mainly ascribed to the maximum sunlight intensity from 11:00 to 15:00 that day, which then basically disappeared at 19:00. The results show that the hanging photothermal fabric-based PANI/CNT has great hydrophilicity, excellent photothermal performance, and good photothermal conversion efficiency. The hanging-mode solar evaporator based on the PANI/CNT fabric shows excellent photothermal performance, photothermal conversion efficiency, and recycling stability, which may provide a novel strategy for the sustainable technique of water purification applications.

CONCLUSIONS

In summary, we designed a hanging-mode solar evaporator based on the PANI/CNT fabric. The PANI/CNT is loaded on the fabric by a simple and scalable dip-coating method. During water evaporation, the photothermal fabric acts as a solar evaporator, and two ends of the fabric act as water transfer channels. The use of an indirect evaporation system with such an interface as a hanging mode is helpful to prevent heat dissipation into bulk water and realize efficient evaporation with the double interface. The results show that the PANI/CNT fabric has great hydrophilicity, excellent photothermal performance, and good photothermal conversion efficiency, with an evaporation rate reaching 2.81 kg·m^{-2}·h^{-1} and a photothermal efficiency reaching 91.74% under a solar illumination of 1 kW·m^{-2}. In addition, the high-performance evaporator is designed by regulating the photothermal material and the evaporation device, which provides a new idea for sustainable desalination.

EXPERIMENTAL SECTION

Materials. Fabrics (thickness: ∼0.5 mm) were purchased from Henan Yujin Textile Co., Ltd. Ammonium persulfate

$((NH_4)_2S_2O_8$, ≥98% purity), hydrochloric acid (HCl, 37 wt %), aniline (≥99.5% purity), ethanol (99.8%), and 3-(trimethoxysilyl)propyl methacrylate (KH-570, ≥98% purity) were purchased from Shanghai Aladdin Biochemical Technology Co., Ltd. Multiwalled carbon nanotube aqueous dispersion (OD: 5−15 nm, 2 wt %) was purchased from Shanghai Titan Scientific Co., Ltd. All the reagents were used as received without any purification.

Characterization. The diffraction spectra of the sample and its composition were performed using the diffraction of X-rays (XRD, DX-2700B, China) with a step angle of 0.06°, a sampling time of 0.5 s, and a scan range of 10−90°. Field-emission transmission electron microscopy (FE-TEM, JEM-F200, Japan) was used to investigate morphologies of the PANI/CNT powder. The scanning electron microscope (SEM, Inspect F50, USA) was used to estimate the surface characteristics of the fabric and PANI/CNT fabric. The water contact angle (CA) was used to estimate the wettability of the fabric and PANI/CNT fabric, which was measured using German-Dataphysics-OCA20. The temperature changes of the PANI/CNT fabric were determined using an infrared thermal imager (HT-19, Hti, China) under infrared irradiation (R95E, Philips, Poland). The ion concentrations of the collected condensed water were analyzed by inductively coupled plasma optical emission spectrometry (ICP-OES, HORIBA Ultima Expert, France).

Preparation of PANI/CNT Powder. Ammonium persulfate (1.141 g) and CNT (0.4 g) were added to hydrochloric acid solution (50 mL, 1 mol·L^{-1}) and stirred well and then cooled to 4 °C in a refrigerator. Next, a solution containing aniline monomer (0.460 mL) and ethanol (1 mL) was added to the above solution, and the solution was kept under magnetic stirring for 105 min in an ice bath. After the low-temperature reaction, the product underwent vacuum filtering for purity, repeatedly washed with deionized water until the filtrate was colorless to remove excess reagents, and dried to obtain PANI/CNT powder.

Preparation of the PANI/CNT Fabric. First, the fabric was soaked in anhydrous ethanol, ultrasonically cleaned for 10

min to remove surface impurities, and dried for use. Next, the prepared PANI/CNT powder was dispersed in an ethanol solution of KH-570 (1 wt %) to prepare a PANI/CNT suspension with a solid content of 5 mg·mL^{-1}. Finally, the pretreated fabric was placed in the suspension for 5 min, then removed, and dried, and the operation was repeated three times to prepare the PANI/CNT fabric.

Water Evaporation Experiments. The water evaporation experiments were carried out indoors at constant temperature (25 ± 1 °C) and humidity (40 ± 5%). Using the hanging mode, the PANI/CNT fabric was placed on the water container, ensuring that both sides were immersed into the container. The thermal area (projected area: 5.0 cm × 4.0 cm) of the PANI/CNT fabric was irradiated by an infrared simulator with light intensity (1 kW·m^{-2}). An electronic balance was used to record the weight changes during evaporation and an infrared thermal imaging camera for recording the temperature change over time.

ASSOCIATED CONTENT

Supporting Information

The Supporting Information is available free of charge at https://pubs.acs.org/doi/10.1021/acsomega.3c05332.

XRD of PANI, CNT, and PANI/CNT; SEM images for the PANI/CNT fabric and powder; infrared images of the PANI/CNT fabric at different $n((NH)_4S_2O_4)/n(An)$ mole ratios and growth times; infrared images of the various fabrics at different times; photothermal efficiency of the PANI/CNT fabric; and quality of the condensed water (PDF)

AUTHOR INFORMATION

Corresponding Author

Yuxin Yang − School of Mechanical Engineering, Chengdu University, Chengdu 610000, PR China; orcid.org/0000-0002-4574-3049; Email: yangyuxin@cdu.edu.cn

Authors

Daiyi Wang − School of Mechanical Engineering, Chengdu University, Chengdu 610000, PR China
Xiaofeng Lin − School of Mechanical Engineering, Chengdu University, Chengdu 610000, PR China
Yujian Wu − School of Mechanical Engineering, Chengdu University, Chengdu 610000, PR China
Luxin Li − School of Mechanical Engineering, Chengdu University, Chengdu 610000, PR China
Wei Feng − School of Mechanical Engineering, Chengdu University, Chengdu 610000, PR China
Yanyan Huang − School of Mechanical Engineering, Chengdu University, Chengdu 610000, PR China

Complete contact information is available at:
https://pubs.acs.org/10.1021/acsomega.3c05332

Notes
The authors declare no competing financial interest.

ACKNOWLEDGMENTS

REFERENCES

(1) Pang, Y.; Zhang, J.; Ma, R.; Qu, Z.; Lee, E.; Luo, T. Solar−Thermal Water Evaporation: A Review. ACS Energy Lett. 2020, 2, 437−456.
(2) Wang, S.; Xiao, C.; Lu, S.; Qu, N.; Hasi, Q.; Zhang, Y.; Chen, L. Aligned Aerogels with High Salt-Resistance and Anti-Biofouling for Efficient Solar Evaporation. J. Environ. Chem. Eng. 2022, 10, No. 108379.
(3) Dao, V. D.; Vu, N. H.; Yun, S. Recent Advances and Challenges for Solar-Driven Water Evaporation System toward Applications. Nano Energy 2020, 68, No. 104324.
(4) Li, J.; Jing, Y.; Xing, G.; Liu, M.; Cui, Y.; Sun, H.; Zhu, Z.; Liang, W.; Li, A. Solar-Driven Interfacial Evaporation for Water Treatment: Advanced Research Progress and Challenges. J. Mater. Chem. A. 2022, 36, 18470−18489.
(5) Jiang, H.; Liu, X.; Wang, D.; Qiao, Z.; Wang, D.; Huang, F.; Peng, H.; Hu, C. Designing High-Efficiency Light-to-Thermal Conversion Materials for Solar Desalination and Photothermal Catalysis. J. Energy Chem. 2023, 79, 581−600.
(6) Fuzil, N. S.; Othman, N. H.; Alias, N. H.; Marpani, F.; Othman, M. H. D.; Ismail, A. F.; Lau, W. J.; Li, K.; Kusworo, T. D.; Ichinose, I.; Shirazi, M. M. A. A Review on Photothermal Material and its Usage in the Development of Photothermal Membrane for Sustainable Clean Water Production. Desalination 2021, 517, No. 115259.
(7) Wu, X.; Chen, G. Y.; Owens, G.; Chu, D.; Xu, H. Photothermal Materials: A key Platform Enabling Highly Efficient Water Evaporation Driven by Solar Energy. Mater. Today Energy 2019, 12, 277−296.
(8) Wang, F.; Li, J.; Bai, W.; Wang, C.; Li, A. Recent Progress on the Solar-Driven Interfacial Evaporation Based on Natural Products and Synthetic Polymers. Sol. RRL 2021, 12, No. 2100475.
(9) Wang, Y.; Wang, C.; Song, X.; Huang, M.; Megarajan, S. K.; Shaukat, S. F.; Jiang, H. Improved Light-Harvesting and Thermal Management for Efficient Solar-Driven Water Evaporation Using 3D Photothermal Cones. J. Mater. Chem. A 2018, 6, 9874−9881.
(10) Zhang, Y.; Xiong, T.; Suresh, L.; Qu, H.; Zhang, X.; Zhang, Q.; Yang, J.; Tan, S. C. Guaranteeing Complete Salt Rejection by Channeling Saline Water Through Fluidic Photothermal Structure Toward Synergistic Zero Energy Clean Water Production and in Situ Energy Generation. ACS Energy Lett. 2020, 5, 3397−3404.
(11) Ding, R.; Meng, Y.; Qiao, Y.; Wu, M.; Ma, H.; Zhang, B. Functionalizing Cotton Fabric via Covalently Grafting Polyaniline for Solar-Driven Interfacial Evaporation of Brine. Appl. Surf. Sci. 2022, 598, No. 153665.
(12) Li, X.; Yue, D.; Liu, F.; Yu, J.; Li, B.; Sun, D.; Ma, X. Acid-Doped Polyaniline Membranes for Solar-Driven Interfacial Evaporation. Korean J. Chem. Eng. 2023, 40, 223−234.
(13) Chen, Z.; Luo, Y.; Li, Q.; Chen, X. Microgroove-Structured PDA/PEI/PPy@ PI-MS Photothermal Aerogel with a Multilevel Water Transport Network for Highly Salt-Rejecting Solar-Driven Interfacial Evaporation. ACS Appl. Mater. Interfaces 2021, 13, 40531−40542.
(14) Ren, X.; Cui, S.; Guan, J.; Yin, H.; Yuan, H.; An, S. PAN@ PPy Nanofibrous Membrane with Core-Sheath Structure for Solar Water Evaporation. Mater. Lett. 2022, 313, No. 131807.
(15) Wang, C.; Wang, Y.; Song, X.; Huang, M.; Jiang, H. A Facile and General Strategy to Deposit Polypyrrole on Various Substrates for Efficient Solar-Driven Evaporation. Adv. Sustainable Syst. 2019, 3, No. 1800108.
(16) Meng, F.; Ding, Z.; Chen, Z.; Wang, K.; Liu, X.; Li, J.; Lu, T.; Xu, X.; Pan, L. N-Doped Carbon@ Cu Core−Shell Nanostructure with Nearly Full Solar Spectrum Absorption and Enhanced Solar Evaporation Efficiency. J. Mater. Chem. A 2022, 10, 9575−9581.
(17) Welegergs, G. G.; Gebretinsae, H. G.; Tsegay, M. G.; Bhardwaj, A.; Mathur, S.; Kebede, T. G.; Nuru, Z. Y.; Dube, S.; Maaza, M. Spectrally Selective Single Layered Ag@ CuO Nanocermet Coatings for Photothermal Application: Green Synthesis Method. Opt. Mater. 2023, 135, No. 113247.

(18) Dong, B.; Wu, X.; Zhan, S.; Nie, G.; Wu, S.; Cheng, S.; Wang, H.; Wu, L.; Liu, Y. Observation of High Efficient Photothermal Conversion of Sub-10 nm Au Nanoparticles Coated on Upconversion Nanoparticles. *Opt. Mater.* **2020**, *101*, No. 109665.

(19) Qu, W.; Zhao, H.; Zhang, Q.; Xia, D.; Tang, Z.; Chen, Q.; He, C.; Shu, D. Multifunctional Au/Ti$_3$C$_2$ Photothermal Membrane with Antibacterial Ability for Stable and Efficient Solar Water Purification under the Full Spectrum. *ACS Sustainable Chem. Eng.* **2021**, *9*, 11372−11387.

(20) Zhu, B.; Kou, H.; Liu, Z.; Wang, Z.; Macharia, D. K.; Zhu, M.; Wu, B.; Liu, X.; Chen, Z. Flexible and Washable CNT-Embedded PAN Nonwoven Fabrics for Solar-Enabled Evaporation and Desalination of Seawater. *ACS Appl. Mater. Interfaces* **2019**, *11*, 35005−35014.

(21) Su, L.; Liu, X.; Li, X.; Yang, B.; Wu, B.; Xia, R.; Qian, J.; Zhou, J.; Miao, L. Facile Synthesis of Vertically Arranged CNTs for Efficient Solar-Driven Interfacial Water Evaporation. *ACS Omega* **2022**, *7*, 47349−47356.

(22) Kang, Y. H.; Bae, E. J.; Lee, M. H.; Han, M.; Kim, B. J.; Cho, S. Y. Highly Flexible and Durable Thermoelectric Power Generator Using CNT/PDMS Foam by Rapid Solvent Evaporation. *Small* **2022**, *18*, No. 2106108.

(23) Li, S.; Qiu, F.; Xia, Y.; Chen, D.; Jiao, X. Integrating a Self-Floating Janus TPC@ CB Sponge for Efficient Solar-Driven Interfacial Water Evaporation. *ACS Appl. Mater. Interfaces* **2022**, *14*, 19409−19418.

(24) Wang, S.; Gao, Z.; Qi, X.; Li, C.; He, L.; Bi, J.; Liu, Z. Superhydrophobic Carbon Black-Loaded Polyurethane Sponge for Efficient Oil-Water Separation and Solar-Driven Cleanup of High-Viscosity Crude Oil. *J. Water Process. Eng.* **2023**, *53*, No. 103812.

(25) Liu, P.; Hu, Y.; Li, X.; Xu, L.; Chen, C.; Yuan, B.; Fu, M. Enhanced Solar Evaporation Using a Scalable MoS2-Based Hydrogel for Highly Efficient Solar Desalination. *Angew. Chem.* **2022**, *134*, No. e202208587.

(26) Yu, Q.; Wang, Q.; Feng, T.; Wang, L.; Fan, Z. A Novel Functionalized MoS2-Based Coating for Efficient Solar Desalination. *Materials* **2023**, *8*, 3105.

(27) Xiong, J.; Yang, Z.; Wu, B.; Li, M.; Min, X. CuS-Enhanced Light-Absorbing Washable Solar Evaporator Based on Polydopamine-cotton Fabric for Efficient Water Purification. *Int. J. Energy Res.* **2022**, *12*, 16979−16990.

(28) Liu, Z.; Zhou, Z.; Wu, N.; Zhang, R.; Zhu, B.; Jin, H.; Zhang, Y.; Zhu, M.; Chen, Z. Hierarchical Photothermal Fabrics with Low Evaporation Enthalpy as Heliotropic Evaporators for Efficient, Continuous, Salt-Free Desalination. *ACS Nano* **2021**, *8*, 13007−13018.

(29) Chen, L.; Mu, X.; Guo, Y.; Lu, H.; Yang, Y.; Xiao, C.; Hasi, Q. MXene-Doped Kapok Fiber Aerogels with Oleophobicity for Efficient Interfacial Solar Steam Generation. *J. Colloid Interface Sci.* **2022**, *626*, 35−46.

(30) Fan, Q.; Wu, L.; Liang, Y.; Xu, Z.; Li, Y.; Wang, J.; Lund, P. D.; Zeng, M.; Wang, W. The Role of Micro-Nano Pores in Iinterfacial Solar Evaporation Systems−A Review. *Appl. Energy* **2021**, *292*, No. 116871.

(31) Colomban, P.; Folch, S.; Gruger, A. Vibrational Study of Short-Range Order and Structure of Polyaniline Bases and Salts. *Macromolecules* **1999**, *32*, 3080−3092.

(32) Wang, A.; Cheng, L.; Chen, X.; Zhao, W.; Li, C.; Zhu, W.; Shang, D. Reduced Graphene Oxide Covalently Functionalized with Polyaniline for Efficient Optical Nonlinearities at 532 and 1064 nm. *Dyes Pigm.* **2019**, *160*, 344−352.

(33) De Heer, W. A.; Bacsa, W. S.; Chatelain, A.; Gerfin, T.; Humphrey-Baker, R.; Forro, L.; Ugarte, D. Aligned Carbon Nanotube Films: Production and Optical and Electronic Properties. *Science* **1995**, *268*, 845−847.

(34) Zhu, L.; Gao, M.; Peh, C. K. N.; Ho, G. W. Recent Progress in Solar-Driven Interfacial Water Evaporation: Advanced Designs and Applications. *Nano Energy* **2019**, *57*, 507−518.

(35) Li, Y.; Shi, Y.; Wang, H.; Liu, T.; Zheng, X.; Gao, S.; Lu, J. Recent Advances in Carbon-Based Materials for Solar-Driven Interfacial Photothermal Conversion Water Evaporation: Assemblies, Structures, Applications, and Prospective. *Carbon Energy* **2023**, No. e331.

(36) Meng, D.; Fan, J.; Ma, J.; Du, S. W.; Geng, J. The Preparation and Functional Applications of Carbon Nanomaterial/Conjugated Polymer Composites. *Compos. Commun.* **2019**, *12*, 64−73.

(37) Liu, H.; Huang, G.; Wang, R.; Huang, L.; Wang, H.; Hu, Y.; Cong, G.; Bao, F.; Xu, M.; Zhu, C.; Xu, J.; Ji, M. Carbon Nanotubes Grown on the Carbon Fibers to Enhance the Photothermal Conversion toward Solar-Driven Applications. *ACS Appl. Mater. Interfaces* **2022**, *14*, 32404−32411.

(38) Primadona, I.; Permatasari, F. A.; Irham, M. A.; Nasir, M.; Iskandar, F. Recent Advances and Rational Design Strategies of Carbon Dots towards Highly Efficient Solar Evaporation. *Nanoscale* **2021**, *13*, 7523−7532.

(39) Wang, S.; Xiao, C.; Lu, S.; Lu, H.; Hasi, Q.; Zhang, Y.; Luo, X.; Chen, L. Integrated Solar Evaporator with Salt Resistance and Lipophobicity Derived from Waste Newspapers for Efficient Desalination. *ACS Sustainable Chem. Eng.* **2023**, *11*, 2586−2598.

(40) Du, C.; Huang, C. A Floating Vapor Condensation Structure in A Heat-Localized Solar Evaporation System for Facile Solar Desalination. *Appl. Therm. Eng.* **2022**, *201*, No. 117834.

(41) Yuan, Z.; Zhang, X.; Zhang, J.; Zhao, X.; Liu, S.; Yu, S.; Liu, X.; Yi, X. Flexible and Robust Nanofiber Sponge with Superior Capacity to Transport Water for Efficient and Sustained Solar-Driven Interfacial Evaporation. *Desalination* **2023**, *550*, No. 116399.

(42) Zhao, L.; Yang, Z.; Wang, J.; Zhou, Y.; Cao, P.; Zhang, J.; Yuan, P.; Zhang, Y.; Li, Q. Boosting Solar-Powered Interfacial Water Evaporation by Architecting 3D Interconnected Polymetric Network in CNT Cellular Structure. *Chem. Eng. J.* **2023**, *451*, No. 138676.

(43) Ge, B.; Tang, S.; Zhang, H.; Li, W.; Wang, M.; Ren, G.; Zhang, Z. Water Vapor Recovery Device Designed with Interface Local Heating Principle and Its Application in Clean Water Production. *J. Mater. Chem. A* **2021**, *9*, 7967−7976.

(44) Yin, X.; Zhang, Y.; Xu, X.; Wang, Y. Bilayer Fiber Membrane Electrospun from MOF Derived Co3S4 and PAN for Solar Steam Generation Induced Sea Water Desalination. *J. Solid State Chem.* **2021**, *303*, No. 122423.

(45) Wang, X.; Jia, P.; Sun, S.; He, X.; Lu, T.; Xu, F.; Feng, S. Evaporation-Induced Diffusion Acceleration in Liquid-Filled Porous Materials. *ACS Omega* **2021**, *33*, 21646−21654.

(46) Xiao, C.; Hasi, Q.; Wang, S.; Zhang, Y.; Li, H.; Zhang, L.; Chen, L.; Li, A. Hollow SiO2 Microspheres in-situ Doped Poly (Ionicliquid) s Gels as Efficient Solar Steam Generators for Desalination. *J. Colloid Interface Sci.* **2022**, *613*, 661−670.

(47) Xia, M.; Wei, J.; Han, Z.; Tian, Q.; Xiao, C.; Hasi, Q. M.; Zhang, Y.; Chen, L. An Integrated Solar Absorber with Salt-Resistant and Oleophobic Based on PVDF Composite Membrane for Solar Steam Generation. *Mater. Today Energy* **2022**, *25*, No. 100959.

(48) Chen, L.; Xia, M.; Du, J.; Luo, X.; Zhang, L.; Li, A. Superhydrophilic and Oleophobic Porous Architectures Based on Basalt Fibers as Oil-Repellent Photothermal Materials for Solar Steam Generation. *ChemSusChem* **2020**, *13*, 493−500.

(49) Kou, H.; Liu, Z.; Zhu, B.; Macharia, D. K.; Ahmed, S.; Wu, B.; Zhu, M.; Liu, X.; Chen, Z. Recyclable CNT-Coupled Cotton Fabrics for Low-Cost and Efficient Desalination of Seawater under Sunlight. *Desalination* **2019**, *462*, 29−38.

(50) Khajevand, M.; Azizian, S.; Jaleh, B. A Bio-Based 3D Evaporator Nanocomposite for Highly Efficient Solar Desalination. *Sep. Purif. Technol.* **2022**, *284*, No. 120278.

(51) Wang, Z.; Huang, H.; Huang, S.; Lin, P.; Pan, D.; Wang, H.; Huang, J.; Wang, L. Continuous and Efficient Purification of Seawater Using Suspended Photothermal Nanocomposite Fabrics with Self-Floatation. *React. Funct. Polym.* **2022**, *175*, No. 105270.

(52) Wei, J.; Xiao, C.; Lu, H.; Jiang, X.; Zhang, Y.; Hasi, Q.; Li, L.; Chen, L. Porous Aerogel with Aligned Hierarchical Channels Based

on Chitosan and Halloysite for Efficient Solar Steam Generation. *Appl. Clay Sci.* **2022**, *229*, No. 106691.

(53) He, M.; Dai, H.; Liu, H.; Cai, Q.; Liu, Y.; Wang, L.; Qin, X.; Yu, J. High-Performance Solar Steam Generator Based on Polypyrrole-Coated Fabric Via 3D Macro-and Microstructure Design. *ACS Appl. Mater. Interfaces* **2021**, *13*, 40664−40672.

(54) Wang, L.; Xi, G.; Chen, Z.; Wang, Q.; Liu, J.; Zhang, R.; Jia, T.; Zhao, X. The Efficient Photothermal Performance of Organic Polymeric Material Poly3-Hexylthiophene for Solar Driven Water Evaporation and Thermoelectric Power Generation. *J. Solid State Chem.* **2023**, *324*, No. 124081.

(55) Yu, Z.; Gu, R.; Tian, Y.; Xie, P.; Jin, B.; Cheng, S. Enhanced Interfacial Solar Evaporation Through Formation of Micro-Meniscuses and Microdroplets to Reduce Evaporation Enthalpy. *Adv. Funct. Mater.* **2022**, *32*, No. 2108586.

(56) Liu, Z.; Wu, B.; Zhu, B.; Chen, Z.; Zhu, M.; Liu, X. Continuously Producing Watersteam and Concentrated Brine from Seawater by Hanging Photothermal Fabrics under Sunlight. *Adv. Funct. Mater.* **2019**, *29*, No. 1905485.

(57) Ai, S.; Wang, Y. N.; Li, T. J.; Chen, Y. Z.; He, C. Y.; Liu, B. H.; Liu, G.; Gao, X. H. A Self-Intensified Inverted Evaporation Model Constructed by High Entropy Spectrally Selective Absorber Coating (SSAC) for Brine Water Concentration. *J. Water Process. Eng.* **2023**, *53*, No. 103814.

(58) Zheng, X.; Ali Mohsin, M. E.; Arsad, A.; Hassan, A. Polymerization of Polyaniline under Various Concentrations of Ammonium Peroxydisulfate and Hydrochloric Acid by Ultrasonic Irradiation. *J. Appl. Polym. Sci.* **2021**, *138*, 50637.

(59) Han, D.; Chu, Y.; Yang, L.; Liu, Y.; Lv, Z. Reversed Micelle Polymerization: A New Route for the Synthesis of DBSA−Polyaniline Nanoparticles. *Colloids Surf., A* **2005**, *259*, 179−187.

(60) Navarchian, H. A.; Hasanzadeh, Z.; Joulazadeh, M. Effect of Polymerization Conditions on Reaction Yield, Conductivity, and Ammonia Sensing of Polyaniline. *Adv. Polym. Technol.* **2013**, *32*, 21356.

(61) Cao, Y.; Andreatta, A.; Heeger, A. J.; Smith, P. Influence of Chemical Polymerization Conditions on the Properties of Polyaniline. *Polymer* **1989**, *30*, 2305−2311.

(62) Ghasemi, H.; Ni, G.; Marconnet, A. M.; Loomis, J.; Yerci, S.; Miljkovic, N.; Chen, G. Solar Steam Generation by Heat Localization. *Nat. Commun.* **2014**, *5*, 4449.

(63) Wu, X.; Robson, M. E.; Phelps, J. L.; Tan, J. S.; Shao, B.; Owens, G.; Xu, H. A Flexible Photothermal Cotton-CuS Nanocage-Agarose Aerogel Towards Portable Solar Steam Generation. *Nano Energy* **2019**, *56*, 708−715.